Supporting Information

# Flash microwave-assisted solvothermal (FMS) synthesis of photoactive anatase sub-microspheres with hierarchical porosity.

**M. Davide Cappelluti,[a,b] Emina Hadzifejzovic, [c] John Foord [c] and Duncan H. Gregory [a] ***

*a. WestCHEM, School of Chemistry, University of Glasgow, University Avenue, Glasgow G12 8QQ, UK*
*b. School of Engineering, University of Glasgow, Oakfield Avenue, Glasgow G12 8LT*
*c. Chemistry Research Laboratory, University of Oxford, Mansfield Road Oxford OX1 3TA, UK*

**Further details concerning the experimental methods**

The size distribution of particle was calculated by measuring the particle diameters from different SEM images at different magnification. As a standard method, at least 100 particles from 5 different image frames were measured for each single sample. The calculation was performed with the software ImageJ (National Institutes of Health, US).

Raman spectroscopy was performed by using laser intensities from 1 - 25 % of the maximum power in order to avoid *in situ* modification (e.g. heating) of the samples (e.g. phase transformations). Raman data were analysed excluding the effect of the Rayleigh scattering and stray light, cutting the spectral region below 75 $cm^{-1}$. Baseline subtraction was then performed by using asymmetric least squares smoothing (with an asymmetric factor of 0.001, a threshold of 0.001 and a smoothing factor variable between 3 and 5 depending on the peak resolution). Baseline subtraction was performed using Origin Pro 2016. Raman peak analysis was performed by using the Fytik software (vs 0.98). Taking the asymmetry between the two sides of the peaks into consideration, the $E_{g\,1}$ peak was fitted with a split-pseudo-Voigt function. The function provided a better fit compared to a conventional pseudo-Voigt alternative or to a combination of multiple Lorentzian-Gaussian functions. The other modes were identified through analysis of the first derivative of the spectra.

Optical band gap calculations were performed using the Kubelka-Munk function F(R):

$$[F(R) \cdot h\nu]^n = \left[\frac{(1-R)^2}{2R} \cdot h\nu\right]^n$$

where *R* is the absolute reflectance and *hν* the photon energy. The intersection with the *x*-axis of the function plotted against the photon energy gives the value of the optical band gap. The exponent n depends on the nature of the optical transition, adopting n = ½ for indirect and n = 2 for direct transitions respectively.

The specific surface area (SSA) was calculated using the BET equation in the interval $0.05 \leq (p/p0) \leq 0.33$. The pore size distribution for mesoporous samples was evaluated by implementation of the BJH equation and DFT calculations, assuming a non-linear approach on the equilibrium isotherms and assuming mixed shape for the pores on a carbonaceous matrix.

The dye concentration before and during the degradation experiment was calculated from the absorption intensity by using a calibration curve based on the linear correlation between concentration and absorption intensity described by the Beer-Lambert law.

**Figures and tables**

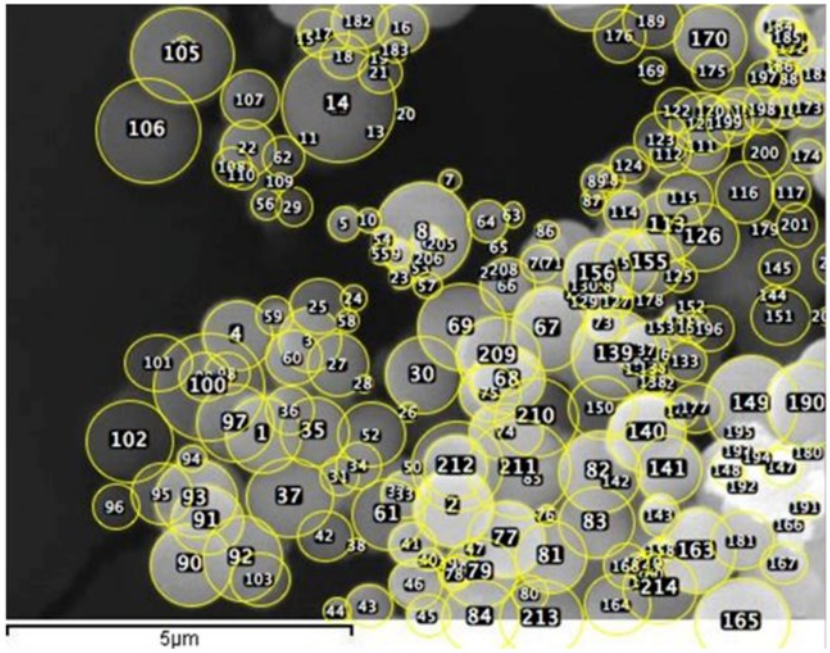


**Figure S1:** Example of SEM image processing for the identification of the particle size distribution by using the ImageJ software. The diameter of all circled particles is calculated from the area, assuming perfect spherical shape for each encircled particle.

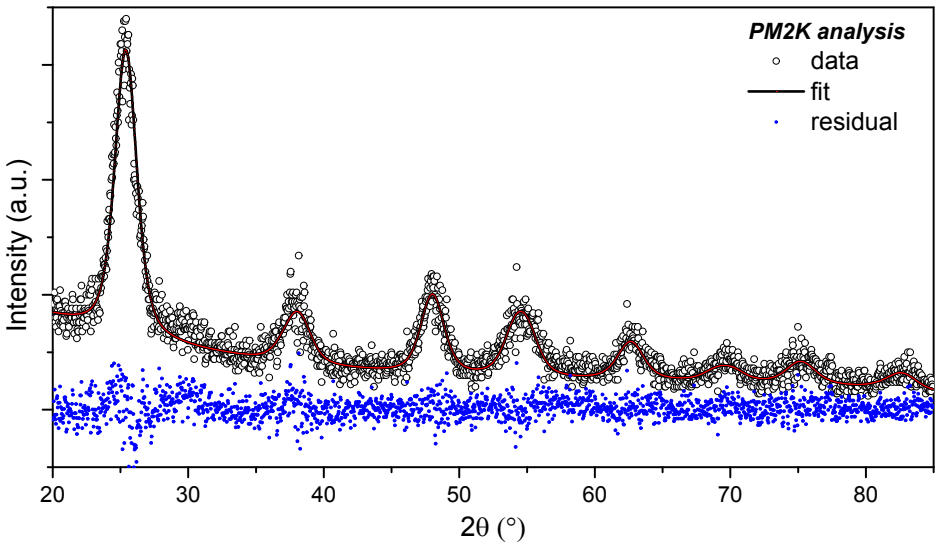


**Figure S2:** Profile fitting of a sample of FMS-$TiO_2$ particles (2M $HNO_3$/160 mM TTIP) using the PM2K software package.[1]

[1] M. Leoni, T. Confente, P. Scardi, Zeitschrift für Kristallographie Supplements, 2006, **23**, 249.

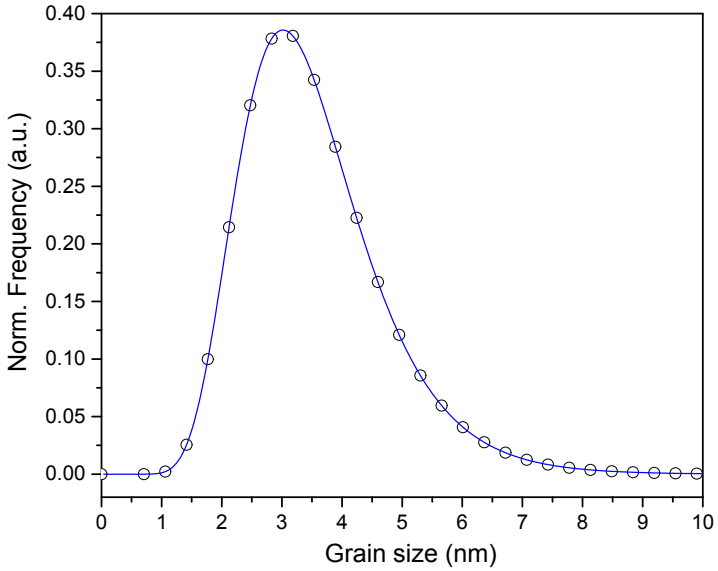


**Figure S3:** Example of the log-normal distribution of the grain size (diameter) estimated using the WPPM method for FMS-$TiO_2$ (2 M $HNO_3$/160 mM precursor concentration; 1 min MW treatment).

**Table S1:** Results of the WPPM refinement and size analysis compared to results obtained from applying the Scherrer equation.

| **FMS-$TiO_2$,** NE series (2 M HNO3, 160 mM TTIP, 1 min MW treatment) | |
|---|---|
| 2θ (101) (°) | 25.292 ± 0.017 |
| FWHM (°) | 1.876 ± 0.017 |
| Scherrer's average grain size (nm) | 4.34 ± 0.04 |
| | |
| **WPPM calculation** | |
| WPPM distribution peak (nm) | 3.35 (3) |
| WPPM distribution width (nm) | 0.33 (4) |
| | |
| **Lattice parameters** | |
| a (Å) | 3.7974(1) |
| c (Å) | 9.4935(94) |
| | |
| **Fitting parameters** | |
| μ | 1.21(8) |
| σ | 0.32(4) |
| No. of variables | 46 |
| No. of observation | 1969 |
| $R_{wp}$ (%) | 16.7 |
| $R_p$ (%) | 18.6 |
| $X^2$ | 0.81 |
| GOF | 0.905 |

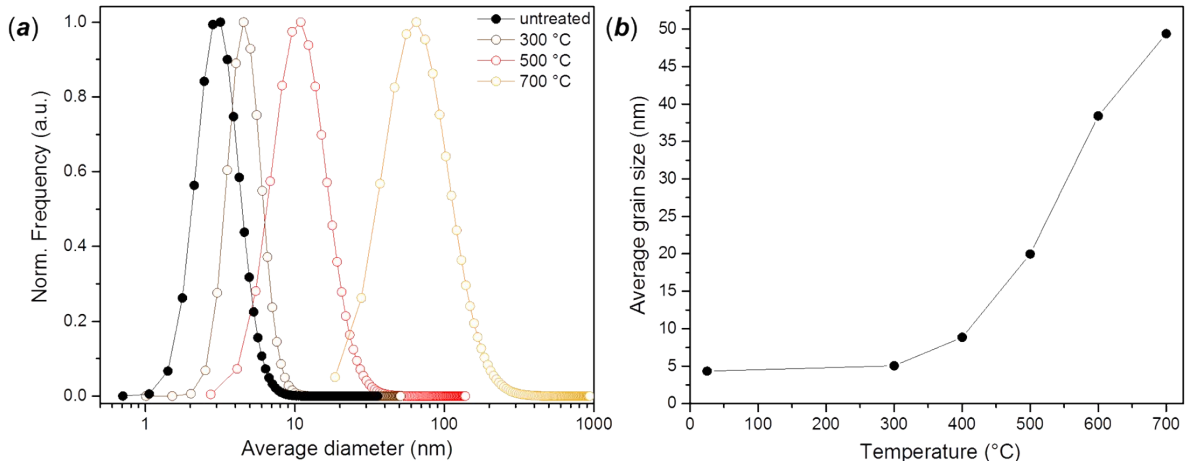


**Figure S4:** Representations of: (a) the lognormal distribution of the crystallite diameter and (b) the average grain size obtained by the WPPM method for a selected sample of FMS $TiO_2$ sub-microspheres (2 M $HNO_3$ concentration/160 mM precursor concentration) as a function of calcination temperature.

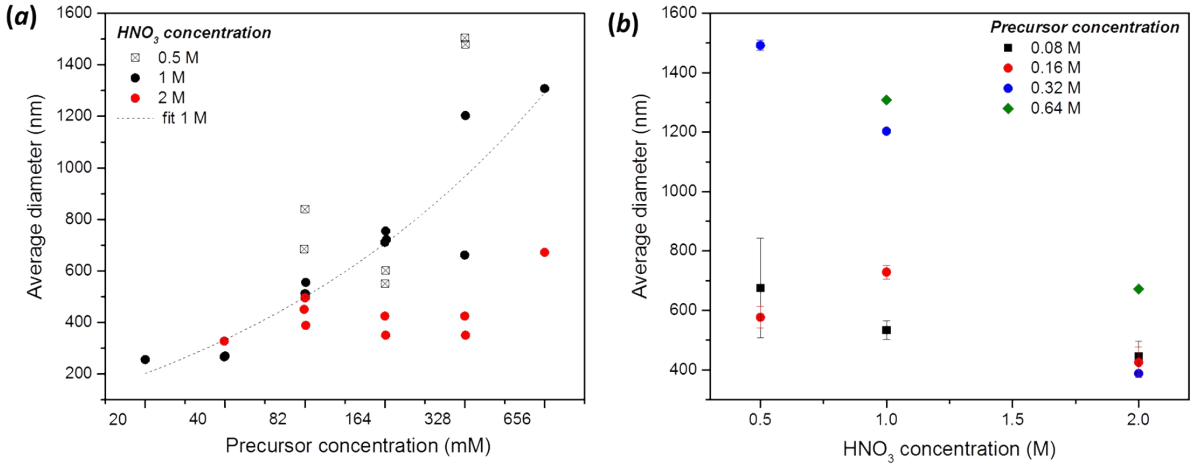


**Figure S5**: Average diameter of selected FMS $TiO_2$ sub-microspheres (from SEM data) as a function of: (a) the precursor concentration and (b) the acid concentration.

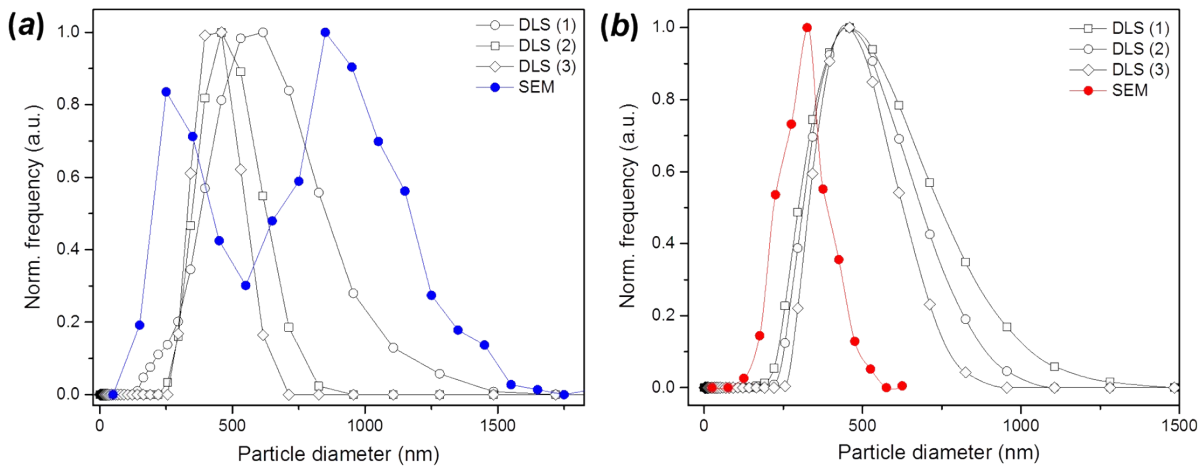


**Figure S6:** Comparison of particle size distributions obtained from SEM particle counting and DLS measurements for different FMS $TiO_2$ sub-microsphere samples; (a) 2 M $HNO_3$/80 mM TTIP concentration samples giving variations in distributions by DLS and a bimodal distribution by SEM; (b) 1 M $HNO_3$/160 mM TTIP concentration samples giving consistent distributions by DLS and a monomodal particle diameter distribution by SEM measurements.

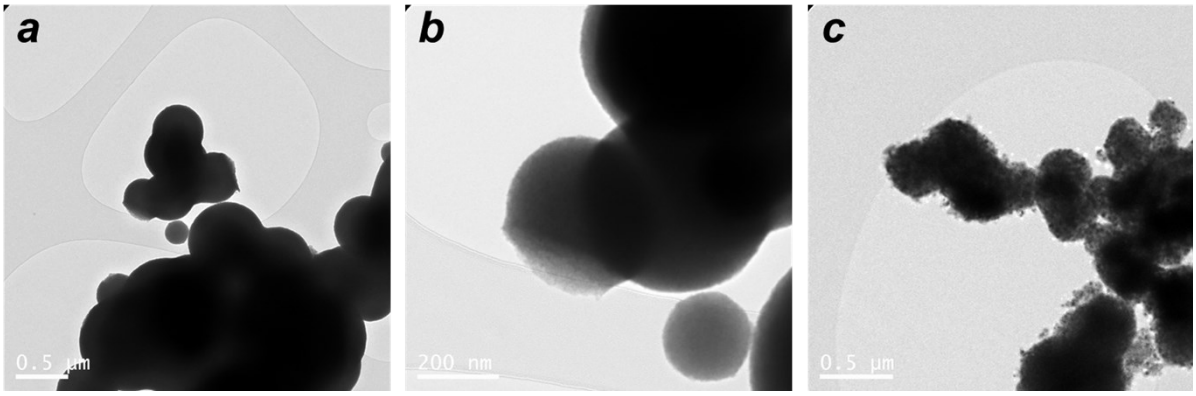


**Figure S7:** TEM images of FMS-$TiO_2$ spheres (2 M $HNO_3$ solution in ethanol/162 mM of TTIP as precursor; 1 min MW treatment): (a),(b) as-synthesised and (c) after calcination treatment (500 °C , 3 h treatment, 5 °C $min^{-1}$ heating rate).

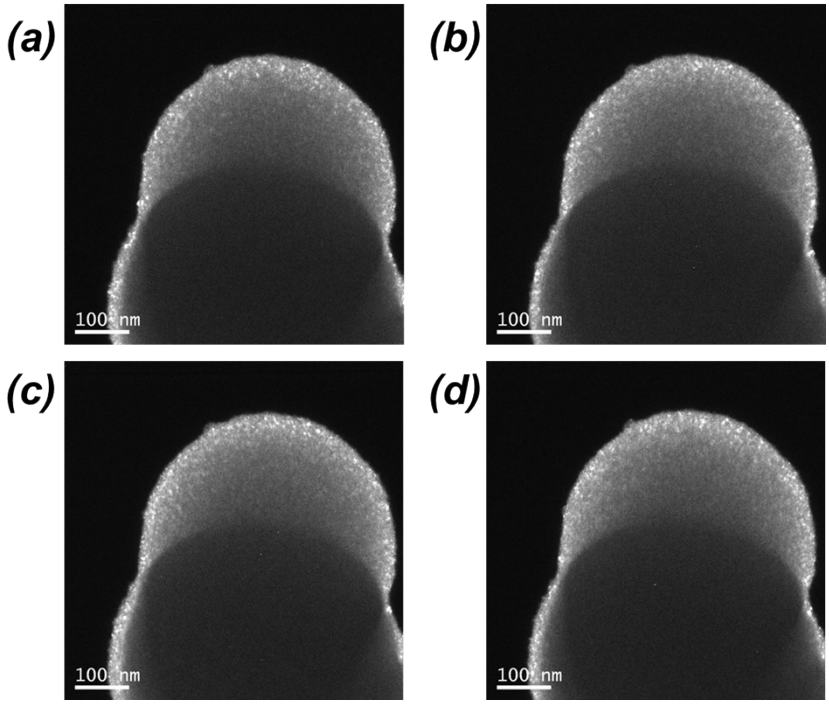


**Figure S8:** HAADF-STEM images of as-synthesised of FMS-$TiO_2$ spheres (2 M $HNO_3$ solution in ethanol/162 mM of TTIP as precursor; 1 min MW treatment) taken at: (a) 0°, (b) 90°, (c) 180° and (d) 270° of rotation.

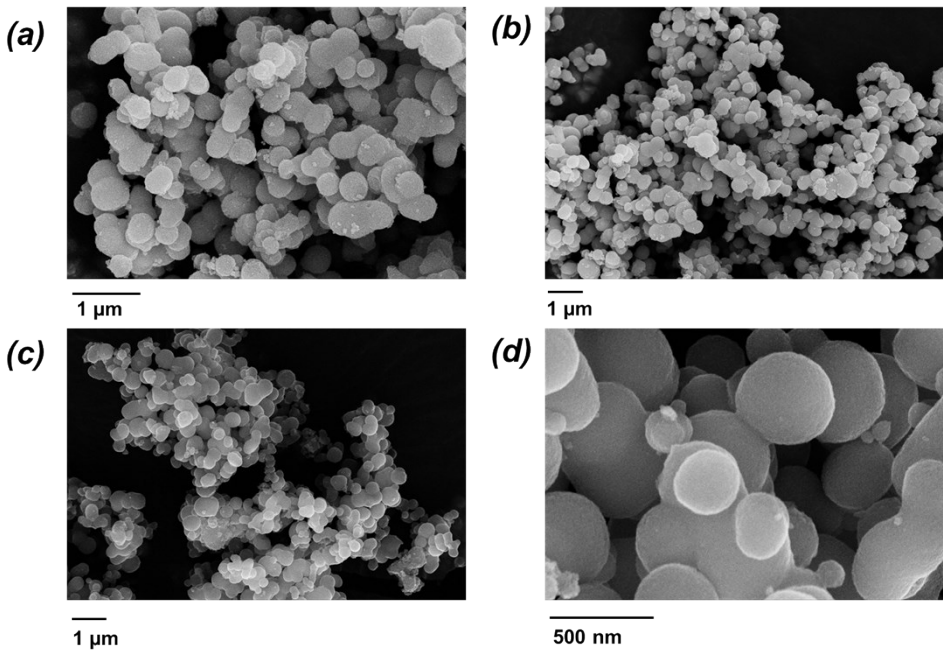


**Figure S9:** HR-SEM images showing examples of FMS $TiO_2$ sub-microspheres (2 M $HNO_3$ in ethanol/160 mM TTIP; 1 min MW irradiation time) following calcination: (a), (b) after 3 h of treatment at 300 °C; (c), (d) after 6 h treatment at 400 °C .

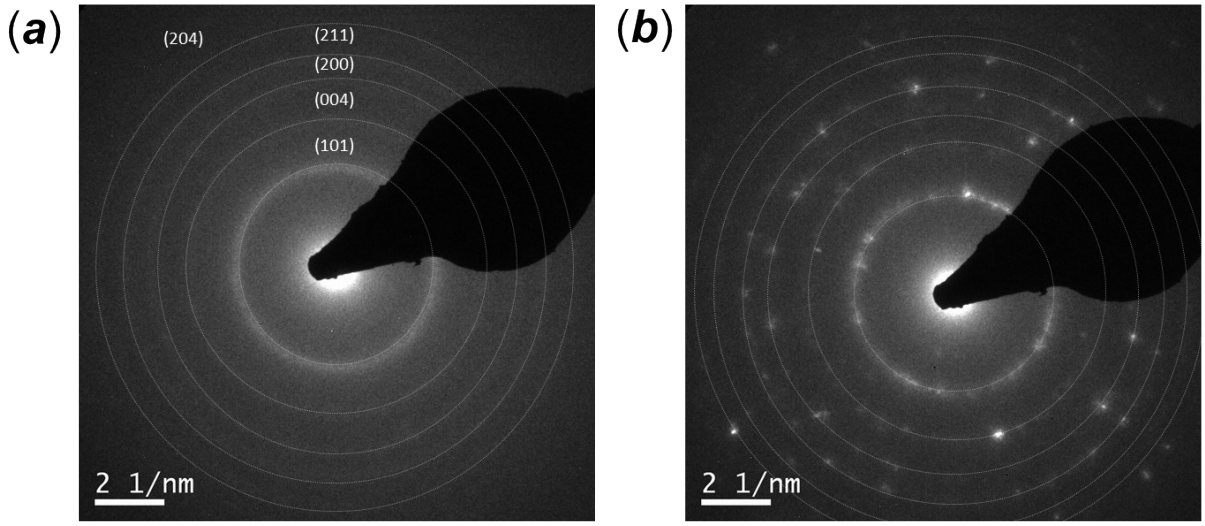


**Figure S10:** SAED images of: (a) untreated FMS $TiO_2$ sub-microspheres (2 M $HNO_3$ in ethanol/ 162 mM TTIP/ 1 min MW irradiation time) and (b) the same sample after calcination at 500 °C for 3 h.

**Table S2:** Assignment of the Raman modes for the spectra shown in Figures 4 and 5 of the manuscript, illustrating the modification of the vibration frequencies and the Eg I mode peak broadening as a function of acid and precursor concentration.

| **Concentration** | | **$E_{g\ I}$ / $cm^{-1}$** | **$E_{g\ I}$ FWHM / $cm^{-1}$** | **$A_{1g}$ / $cm^{-1}$** | **$B_{1g}$ / $cm^{-1}$** | **$E_{g\ III}$ / $cm^{-1}$** |
|---|---|---|---|---|---|---|
| *Acid* | *0.5 M* | 152.6 | 25.7 | 398.5 | 516.3 | 647.5 |
| | *1 M* | 152.4 | 24.2 | 396.8 | 517.0 | 647.0 |
| | *2 M* | 151.0 | 22.8 | 398.1 | 518.4 | 644.7 |
| *Precursor* | *20 mM* | 152.9 | 65.1 | 422.9 | 519.9 | 626.0 |
| | *40 mM* | 152.9 | 41.4 | 409.8 | 515.9 | 636.7 |
| | *80 mM* | 147.4 | 25.7 | 393.7 | 510.9 | 636.9 |
| | *160 mM* | 147.9 | 22.9 | 392.7 | 514.4 | 640.0 |
| | *320 mM* | 148.3 | 23.3 | 394.5 | 514.5 | 642.3 |
| | *650 mM* | 148.3 | 24.3 | 392.4 | 512.1 | 639.2 |

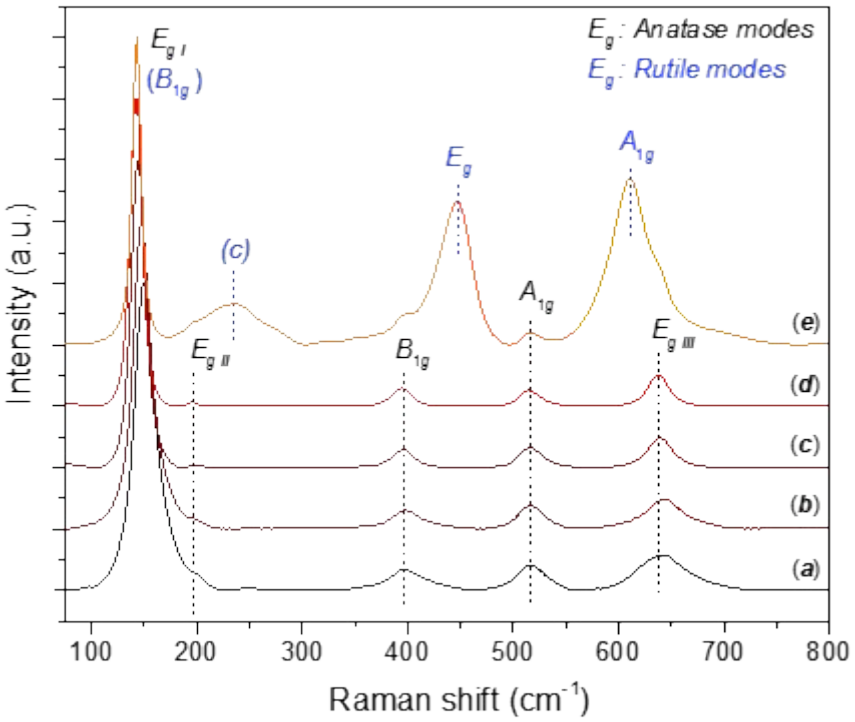


**Figure S11**: Raman spectra of FMS $TiO_2$ sub-microparticles (2 M $HNO_3$/162 mM TTIP precursor concentration; 1 min MW treatment): (a) untreated particles and after calcination (3 h; 5 °C min$^{-1}$ heating rate) at: (b) 300 °C, (c) 400 °C; (d) 500 °C; (e) 600 °C. Characteristic modes for anatase (black) and rutile (blue) phases are marked in the figure.

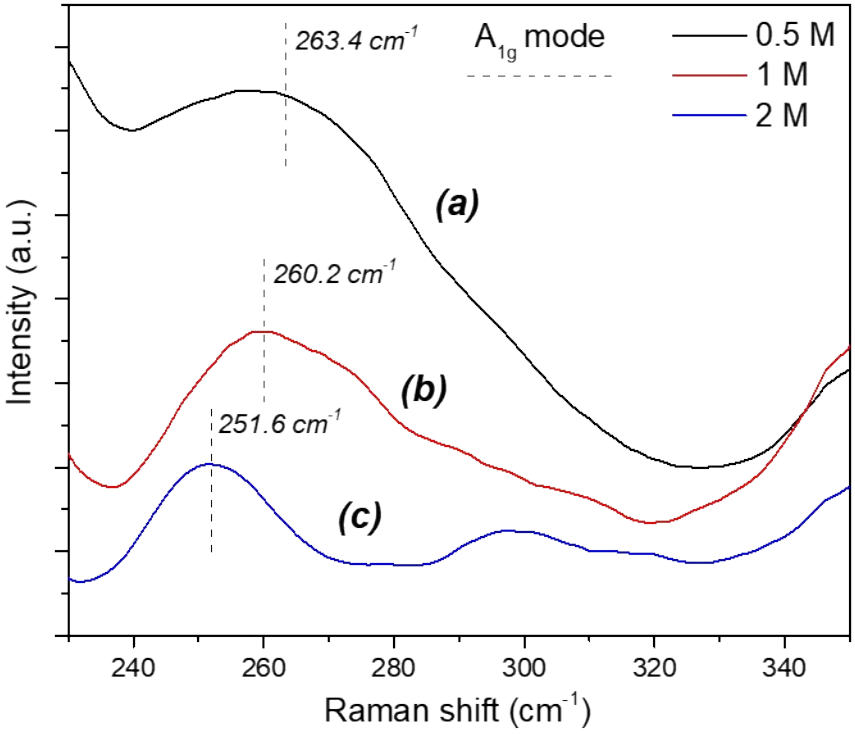


**Figure S12:** Magnification of the 240-340 cm$^{-1}$ Raman spectral region for FMS $TiO_2$ sub-microsphere samples, prepared by using different $HNO_3$ concentration: (***a***) 0.5 M; (***b***) 1 M and (***c***) 2 M; all samples prepared with 160 mM TTIP and 1 min MW irradiation time. No anatase or rutile modes are present in this region and a band from the $A_{1g}$ Raman mode associated with the Brookite phase of $TiO_2$ can be identified (dashed line).

**Table S3:** Specific surface area (SSA), pore size distribution, crystallite size (as estimated by the Scherrer equation), BET diameter and sub-microsphere diameter (from SEM) for selected FMS $TiO_2$ sub-microsphere samples. (The MW irradiation time was set at 1 min for all samples).

| $[HNO_3]$, [TTIP] / M | Isotherm type | BET SSA / $m^2 g^{-1}$ | BJH pore radius / Å | BJH pore vol / $cm^3 g^{-1}$ | Crystallite[a] size / nm | BET diameter[b] / nm | SEM diameter / nm |
|---|---|---|---|---|---|---|---|
| **0.5, 0.08** | I | 251.5 ± 20.6 | 14.9 ± 3.7 | 0.022 ± 0.007 | 3.5 | 6.1 ± 0.5 | 1165 ± 379† |
| **0.5, 0.32** | I | 159.7 ± 15.4 | 17.5 ± 2.4 | 0.060 ± 0.011 | 2.7 | 9.6 ± 0.9 | 1492 ± 566† |
| **1, 0.02** | II | 55.7 ± 6.2 | 14.8 ± 3.9 | 0.014 ± 0.006 | 4.6 | 27.6 ± 1.6 | 265 ± 59 |
| **1, 0.04** | II | 106.2 ± 12.1 | 14.9 ± 3.9 | 0.049 ± 0.009 | 3.8 | 16.4 ± 1.7 | 264 ± 59 |
| **1, 0.16** | I | 214.2 ± 13.6 | 16.6 ± 2.5 | 0.014 ± 0.005 | 5.6 | 7.2 ± 0.5 | 730 ± 273 |
| **1, 0.65** | I | 251.1 ± 15.0 | 15.9 ± 1.9 | 0.011 ± 0.002 | 3.0 | 6.1 ± 0.4 | 1308 ± 740 |
| **2, 0.08** | IV | 510.1 ± 31.5 | 17.9 ± 3.5 | 0.642 ± 0.045 | 4.7 | 3.0 ± 0.2 | 294 ± 93 |
| **2, 0.16** | IV | 369.4 ± 17.4 | 17.5 ± 3.1 | 0.154 ± 0.011 | 3.8 | 4.2 ± 0.2 | 496 ± 230 |
| **2, 0.65** | IV | 507.4 ± 28.4 | 17.9 ± 2.7 | 0.316 ± 0.028 | 3.7 | 3.0 ± 0.2 | 672 ± 230 |

[a] ± 0.1 nm; [b] estimated from surface area assuming spherical particles with homogeneous size distribution; †multimodal distribution.

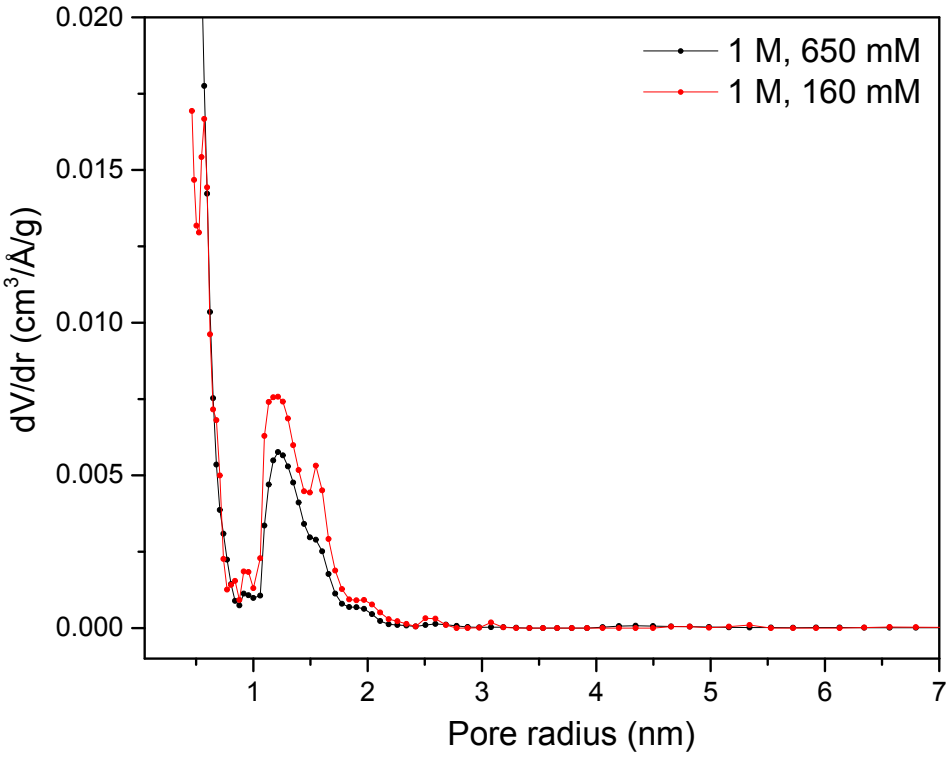


**Figure S13:** Pore size distribution of FMS $TiO_2$ sub-microspheres (1 M $HNO_3$/160 mM TTIP; 1 min MW treatment - red and 1 M $HNO_3$/650 mM TTIP; 1 min MW treatment - black) as calculated by the Quasi-Solid Density Functional Theory (QSDFT) method.

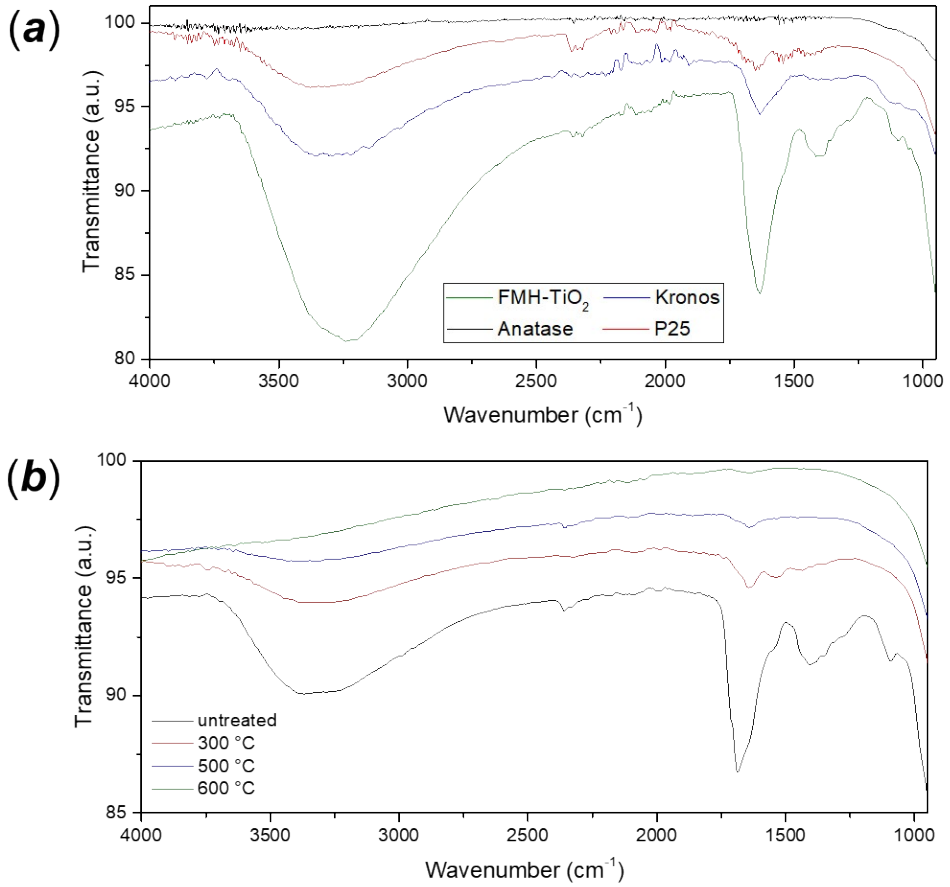


**Figure S14:** (a) IR spectrum of a representative sample of FMS $TiO_2$ sub-microspheres (2M $HNO_3$/160 mM TTIP ; 1 min MW treatment - green) as compared with commercial anatase (black) and the commercial $TiO_2$-based catalysts, P25 (red) and Kronos (blue); (b) IR spectra of FMS $TiO_2$ sub-microspheres (2M $HNO_3$/160 mM TTIP ; 1 min MW treatment) calcined for 3 h at different temperatures (untreated – black; 300 °C – red; 500 °C – blue; 600 °C – green).

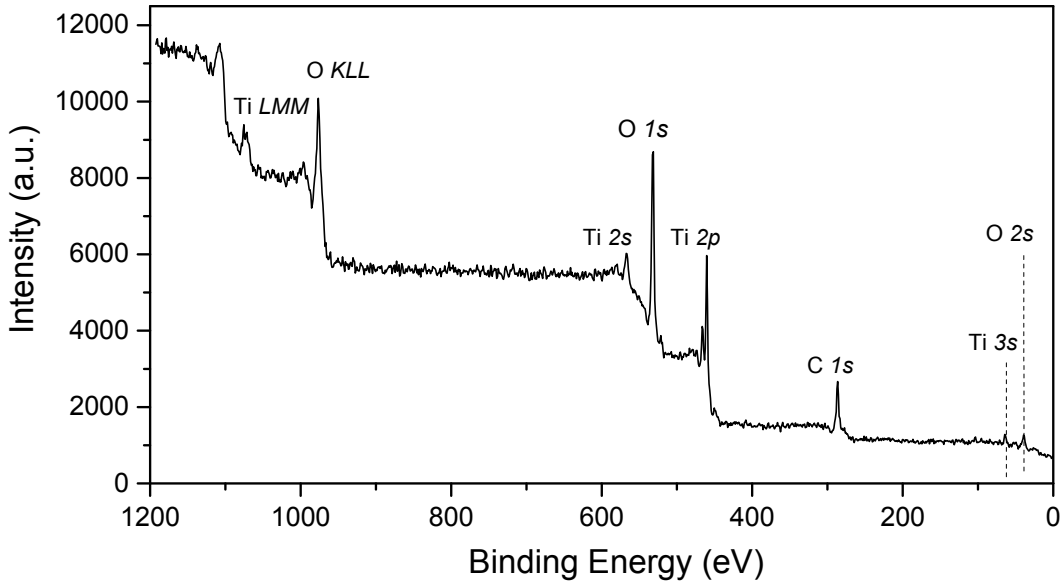


**Figure S15:** Complete XPS spectra of a representative sample of FMS $TiO_2$ sub-microspheres (2 M $HNO_3$/162 mM TTIP; 1 min MW irradiation time).

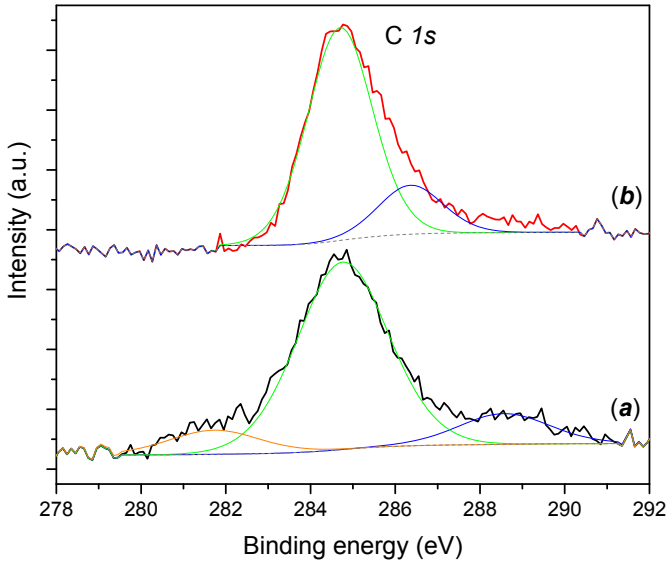

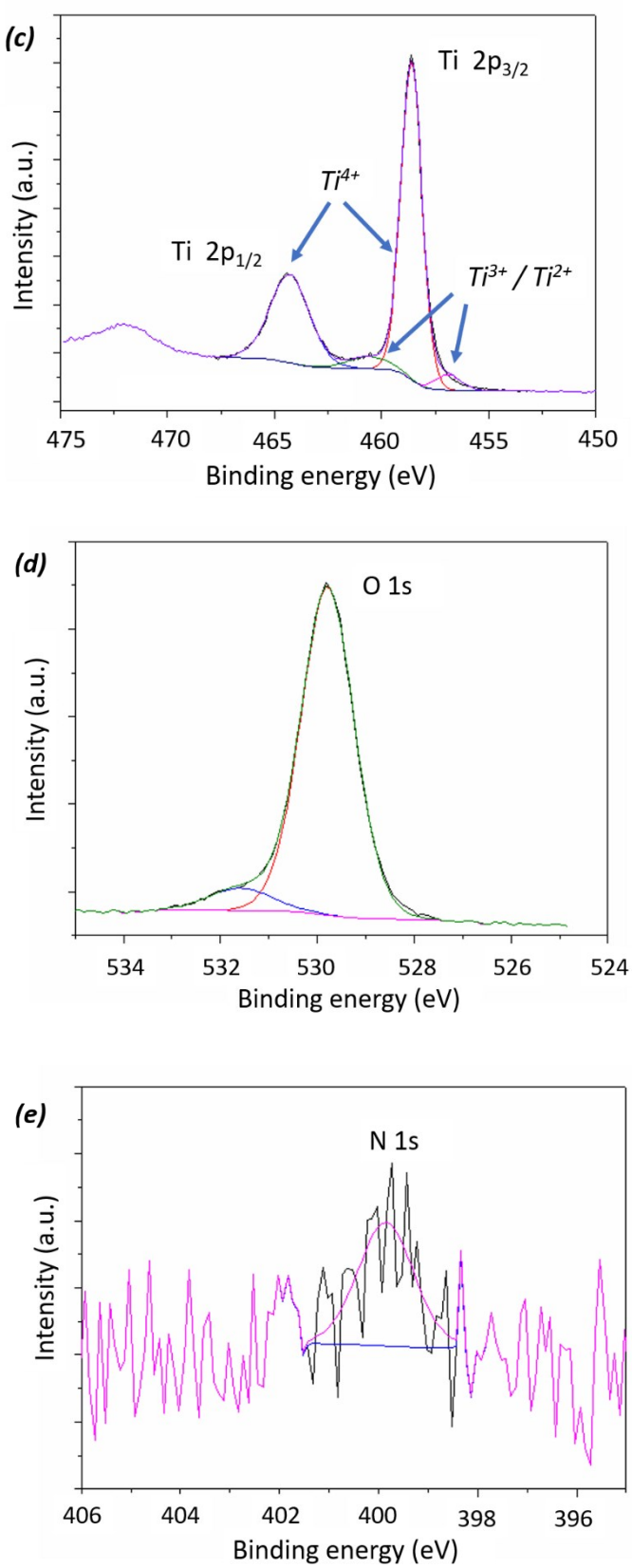


**Figure S16:** Comparison between: (a) the XPS C 1s signal of FMS $TiO_2$ sub-microspheres (2 M $HNO_3$/160 mM TTIP; 1 min MW treatment) and (b) the analogous signal from a sample of Aeroxide P25 (after thermal treatment at 500 °C for other research purposes); Fitted narrow scan XPS spectra of: (c) Ti 2p; (d) O 1s and (e) N 1s peaks from the same sample of FMS $TiO_2$ sub-microspheres shown in (a).

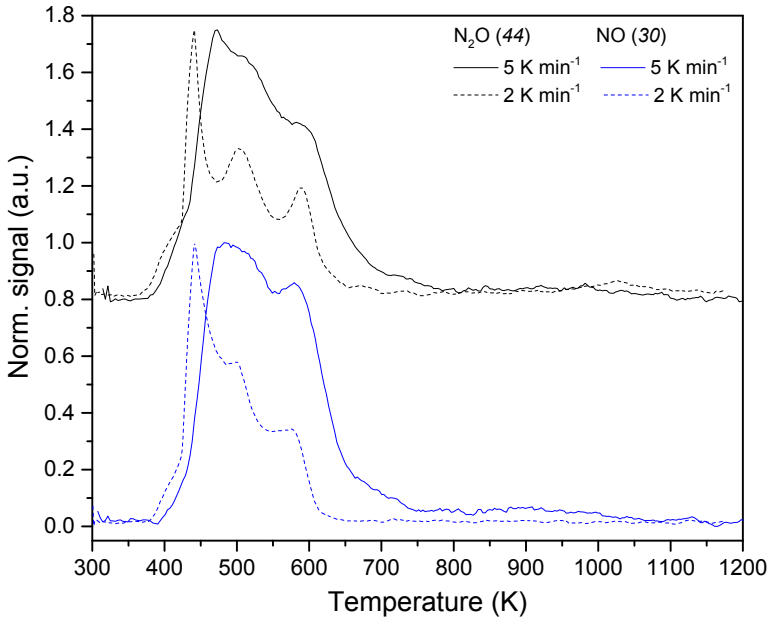


**Figure S17:** Evolved gas MS analysis of the signals tentatively assigned to $N_2O$ (m/z = 44) and NO (m/z = 30) for a selected FMS-$TiO_2$ sub-microsphere sample (2 M $HNO_3$/324 mM TTIP; 1 min MW irradiation time) as a function of temperature and at different heating rates.

**Table S4:** C, H, N combustion microanalysis for selected FMS $TiO_2$ sub-microspheres (1 min MW irradiation time for all samples).

| | **Elements / wt.%** | | |
|---|---|---|---|
| **Sample** | **C** | **H** | **N** |
| **[$HNO_3$], [TTIP] / M** | | | |
| 2, 0.64 | 2.32 ± 0.09 | 0.96 ± 0.04 | 1.32 ± 0.12 |
| 2, 0.16 | 3.09 ± 0.14 | 1.20 ± 0.05 | 0.78 ± 0.06 |
| 1, 0.08 | 2.11± 0.00 | 1.43 ± 0.07 | 0.17 ± 0.00 |
| 0.5, 0.080 | 3.37± 0.06 | 2.28 ± 0.15 | 1.07 ± 0.07 |
| 1, 0.040 | 1.94 ± 0.07 | 2.09 ± 0.07 | 0.17 ± 0.00 |

**Table S5**: Elemental content of FMS $TiO_2$ sub-microspheres (2 M $HNO_3$ solution/ 160 mM TTIP ; 1 min MW treatment) by XPS analysis (at.%) at the surface and at depths of 1 and 10 nm (by Ar etching).

| Element peak | Elemental content / at.% Surface | Depth profile at 1 nm | Depth profile at 10 nm |
|---|---|---|---|
| Ti 2p | 15.15 | 18.86 | 20.93 |
| O 1s | 47.70 | 56.74 | 58.74 |
| C 1s | 37.15 | 23.57 | 20.00 |
| N 1s | - | 0.83 | 0.33 |

**Table S6:** Examples of experimental indirect and direct band gap values as a function of the synthesis conditions of selected FMS $TiO_2$ sub-microspheres (1 min MW irradiation time for all the samples).

| | **[$HNO_3$] / M** | **[TTIP] / M** | **Indirect band gap / eV** | **Direct band gap / eV** |
|---|---|---|---|---|
| Anatase | | | 3.23 | 3.47 |
| FMS sub-microspheres | 0.5 | 0.08 | 3.33-3.36 | 3.65-3.68 |
| | | 0.16 | 3.29-3.31 | 3.68-3.70 |
| | | 0.32 | 3.24-3.27 | 3.62-3.68 |
| | 1 | 0.04 | 3.45 | 3.76-3.80 |
| | | 0.08 | 3.37-3.40 | 3.72-3.74 |
| | | 0.16 | 3.27-3.35 | 3.67-3.73 |
| | 2 | 0.04 | 3.41-3.42 | 3.75-3.76 |
| | | 0.08 | 3.41 | 3.77 |
| | | 0.16 | 3.35-3.41 | 3.72-3.75 |
| | | 0.32 | 3.33-3.36 | 3.66-3.70 |
| | | 0.66 | 3.33 | 3.67 |

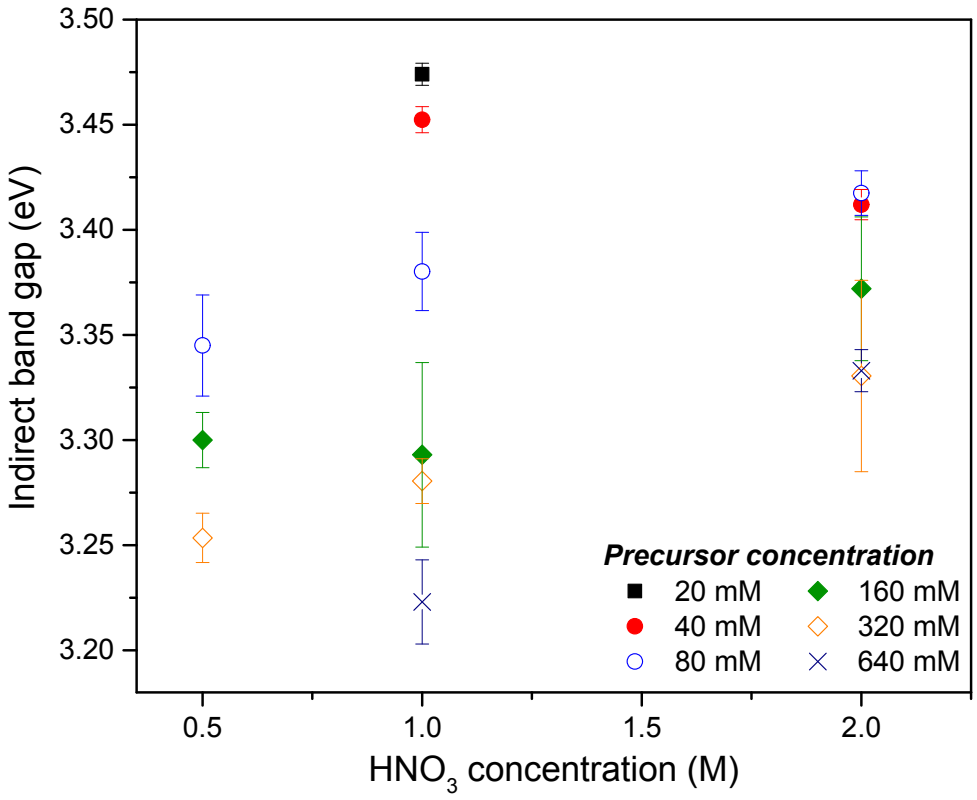


**Figure S18:** Indirect band gap as a function of the acid concentration for the synthesis of FMS $TiO_2$ sub-microspheres. The data are correlated with the precursor (TTIP) concentration used for the preparation of the $TiO_2$ particle. All samples were subjected to 1 min of MW irradiation time.

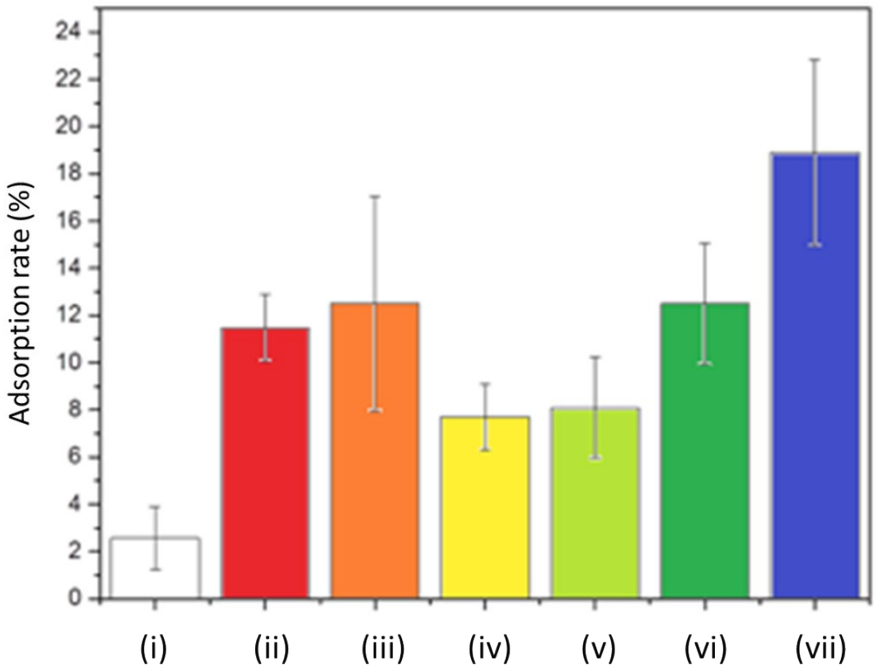


**Figure S19:** Initial adsorption for selected as-synthesised FMS-$TiO_2$ samples as compared to: (i) Aeroxide P25; (ii) 1M $HNO_3$/40 mM TTIP; (iii) 1M HCl/160 mM TTIP; (iv) 2M $HNO_3$/160 mM TTIP; (v) 2M $HNO_3$ (in water)/160 mM TTIP; (vi) 1M $HNO_3$/80 mM TTIP; (vii) 0.5M $HNO_3$/80 mM TTIP. All samples were subjected to 1 min of MW irradiation time.

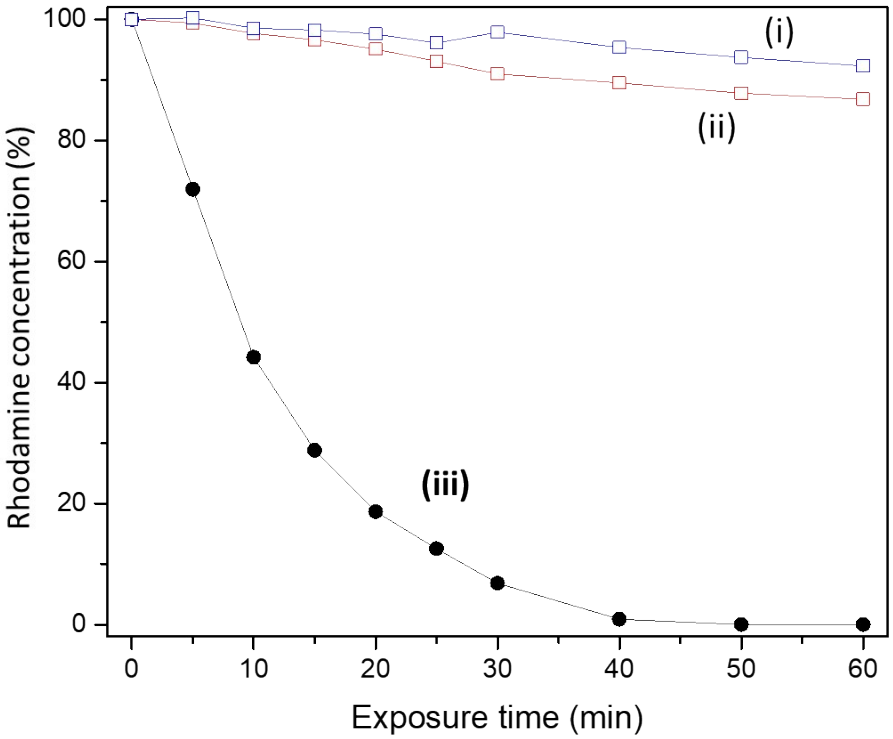


**Figure S20** Degradation curves for selected FMS-$TiO_2$ sub-microsphere samples under UVA light: (i) 1M $HNO_3$/ 40 mM TTIP and (ii) 2M $HNO_3$/320 mM TTIP (1 min MW irradiation time for both samples) as compared to: (iii) Aeroxide P25.


**Figure S21:** Image of the appearance of Rhodamine solution samples following degradation experiments performed using selected FMS $TiO_2$ sub-microspheres under visible light: (a) 0.5M $HNO_3$/160 mM TTIP and (b) 1M $HNO_3$/40 mM TTIP. All samples were subjected to 1 min of MW irradiation time.

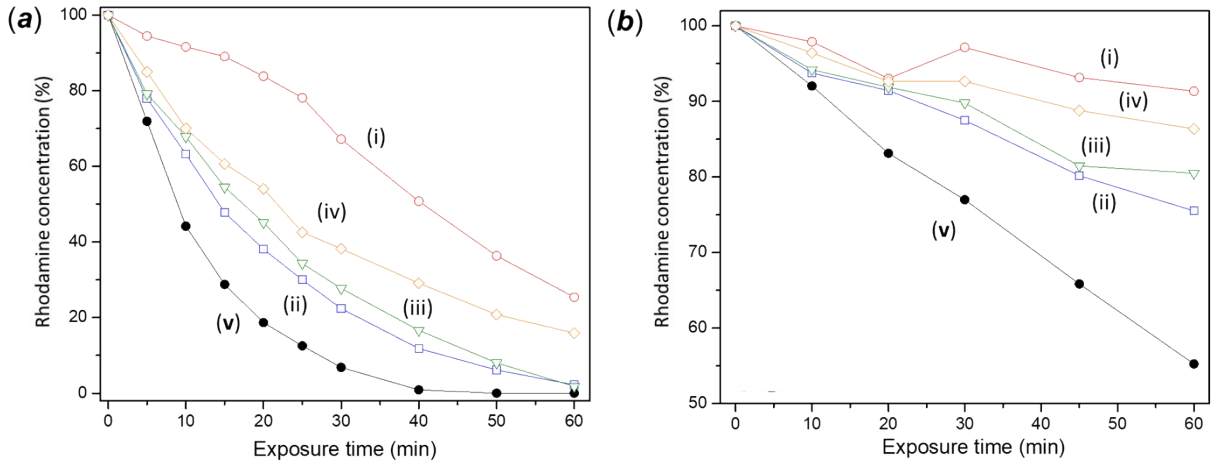


**Figure S22:** Degradation curves under: (a) UVA and (b) visible light for selected FMS $TiO_2$ sub-microspheres calcined in air (3h, 10 °C $min^{-1}$) at different calcination temperatures. The samples shown are: (i) 2M $HNO_3$/160 mM TTIP/400 °C, (ii) 2M $HNO_3$/160 mM TTIP/500 °C, (iii) 2M $HNO_3$/160 mM TTIP/300 °C; (iv) 2M $HNO_3$,320 mM TTIP/500 °C; (v) Aeroxide P25 (included as a comparison). All samples were subjected to 1 min of MW irradiation time.

**Table S7:** Zeta potential results taken from dispersions of FMS $TiO_2$ sub-microspheres produced under different synthesis conditions (all samples were prepared using 160 mM of TTIP as precursor and 2 M $HNO_3$).

| **Synthesis parameters** ***(solvent/MW irradiation time/as made or calcination temperature)*** | **Dispersion Concentration / mg $L^{-1}$** | **Zeta Potential / mV** | **Mobility / µm·cm V $s^{-1}$** | **Conductivity / mS $cm^{-1}$** |
|---|---|---|---|---|
| *Ethanol/30s/as made* | 10mg/L | -28.57 | -2.24 | 0.01 |
| *Ethanol/30s/as made* | 50mg/L | -25.40 | -1.99 | 0.03 |
| *Ethanol/1 min/as made* | 1mg/L | -35.13 | -2.75 | 0.01 |
| *Ethanol/1 min/as made* | 10mg/L | -27.97 | -2.19 | 0.02 |
| *Ethanol/1 min/as made* | 50mg/L | -23.33 | -1.83 | 0.02 |
| *Ethanol/1 min/300 °C* | 10mg/L | -27.73 | -2.18 | 0.01 |
| *Ethanol/1 min/400 °C* | 10mg/L | -17.84 | -1.40 | 0.02 |
| *Ethanol/1 min/500 °C* | 10mg/L | -16.02 | -1.26 | 0.02 |
| *Water/1 min/ as made* | 10mg/L | -23.97 | -1.88 | 0.02 |
| *Water/1 min/as made* | 50mg/L | -19.03 | -1.49 | 0.01 |
| *Water/1 min/300 °C* | 50 mg/L | -23.78 | -1.86 | 0.02 |